

## An Acoustofluidic Micromixer via Bubble Inception and Cavitation from Microchannel Sidewalls

Adem Ozcelik,<sup>†</sup> Daniel Ahmed,<sup>†</sup> Yuliang Xie,<sup>†,‡</sup> Nitesh Nama,<sup>†</sup> Zhiguo Qu,<sup>§</sup> Ahmad Ahsan Nawaz,<sup>†</sup> and Tony Jun Huang<sup>\*,†,‡</sup>

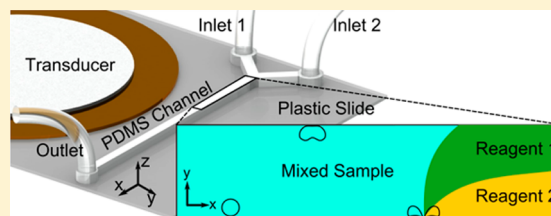
<sup>†</sup>Department of Engineering Science and Mechanics, The Pennsylvania State University, University Park, Pennsylvania 16802, United States

<sup>‡</sup>Department of Chemical Engineering, The Pennsylvania State University, University Park, Pennsylvania 16802, United States

<sup>§</sup>MOE Key Laboratory of Thermal Fluid Science and Engineering, School of Energy and Power Engineering, Xi'an Jiaotong University, Xi'an, Shaanxi 710049, P.R. China

### Supporting Information

**ABSTRACT:** During the deep reactive ion etching process, the sidewalls of a silicon mold feature rough wavy structures, which can be transferred onto a polydimethylsiloxane (PDMS) microchannel through the soft lithography technique. In this article, we utilized the wavy structures of PDMS microchannel sidewalls to initiate and cavitate bubbles in the presence of acoustic waves. Through bubble cavitation, this acoustofluidic approach demonstrates fast, effective mixing in microfluidics. We characterized its performance by using viscous fluids such as poly(ethylene glycol) (PEG). When two PEG solutions with a resultant viscosity 54.9 times higher than that of water were used, the mixing efficiency was found to be 0.92, indicating excellent, homogeneous mixing. The acoustofluidic micromixer presented here has the advantages of simple fabrication, easy integration, and capability to mix high-viscosity fluids (Reynolds number:  $\sim 0.01$ ) in less than 100 ms.



Effective mixing of high-viscosity liquids is important in many fields including chemical synthesis,<sup>1–3</sup> biochemical reactions,<sup>4–7</sup> and clinical diagnosis.<sup>8–14</sup> For example, to study the functions of biomacromolecules in living cells, substrates and enzymes/proteins need to be dissolved in high-viscosity liquids and homogeneously mixed before the enzymatic reaction takes place.<sup>10,15</sup> In the context of clinical diagnostics, high-viscosity body fluids, such as sputum,<sup>16</sup> plasma,<sup>11</sup> or semen,<sup>17</sup> have to be mixed with chemical reagents and/or buffers before performing analysis. In these applications, microfluidic platforms offer many advantages such as small sample/reagent consumption, rapid and high-precision analysis, and low-cost devices.<sup>18–20</sup> On the other hand, achieving effective mixing of viscous samples in microfluidics is challenging due to the extremely low Reynolds number (high viscosity and small channel dimensions).<sup>21–26</sup>

In the past decade, various microfluidic mixers have been developed. These mixers utilize passive approaches, such as diffusion driven<sup>27</sup> and chaotic advection,<sup>28–35</sup> as well as active approaches, such as thermal,<sup>36</sup> optical,<sup>37</sup> magnetic,<sup>38,39</sup> electrokinetic,<sup>40–42</sup> hydrodynamic,<sup>43,44</sup> and acoustic-based<sup>45–53</sup> mixing. However, few of these methods have demonstrated the ability to mix high-viscosity fluids,<sup>54,55</sup> and their performance is often less than optimum. For example, Li et al. used a passive mixer to mix high-viscosity solutions (the highest viscosity is 35.25 mPa s) with a low-viscosity borate buffer solution.<sup>55</sup> The Reynolds number in this mixing device, when achieving homogenous mixing, was reported to be 73.27. Wang et al.

used an acoustic field to generate and oscillate bubbles in circular-geometry channels and induced mixing of water-glycerol solutions, but the mixing was slow (mixing time: 2–4 s).<sup>54</sup> In this regard, it is essential to develop a new class of microfluidic mixers that can achieve effective, fast mixing of high-viscosity fluids with simple devices and experimental setups.

In this work, we present an acoustofluidic (i.e., fusion of acoustics and microfluidics)<sup>56–58</sup> method that takes advantage of the wavy structures in polydimethylsiloxane (PDMS) microchannels made from silicon molds, which were fabricated using the deep reactive ion etching (DRIE) process. Our method exploits the surface roughness of the PDMS microchannel sidewalls to inception and cavitate bubbles in the presence of acoustic waves to achieve rapid mixing of two viscous fluids with excellent homogenization. It achieves fast, homogeneous mixing of high-viscosity fluids (Reynolds number:  $\sim 0.01$ ) without involving any complex device designs or experimental setups. With its simplicity and excellent performance, the acoustofluidic micromixer presented here could become a valuable component in many lab-on-a-chip applications.

Received: February 27, 2014

Accepted: April 22, 2014

Published: April 22, 2014



## EXPERIMENTS

PDMS microchannels with a width, depth, and length of 240  $\mu\text{m}$ , 155  $\mu\text{m}$ , and 1.2 cm were fabricated using standard soft lithography and replica-molding techniques.<sup>59</sup> The microchannel was treated with oxygen plasma and bonded onto a Petri dish. An acoustic sandwich transducer with a diameter of 40 mm and a height of 55 mm (APC, Mackeyville) was bonded onto the same Petri dish using epoxy and placed adjacent to the microchannel. The transducer had a resonant frequency of 120 kHz. Acoustic waves were generated by the transducer driven by a function generator (Hewlett-Packard 8116A) and amplified by a power amplifier (Amplifier Research 100A250A). The whole setup was mounted on an inverted Nikon TE-2000U optical microscope stage. A Nikon Intense-light C-HGFI light source with blue excitation filter block B-2E/C (excitation filter wavelength: 465–495 nm) was used for excitation. Different flow rates ranging from 1  $\mu\text{L}/\text{min}$  to 30  $\mu\text{L}/\text{min}$  were used in the experiments. Deionized (DI) water and fluorescein dye solution were first used for proof-of-concept characterizations. Following that, PEG solutions (molecular weight: ~700 Da) of various viscosities (21.2–95.9 mPa s) and DI water were used in the mixing experiments. In all of our experiments, the frequency and voltage applied were fixed at 38.9 kHz and 160 V (peak to peak), respectively. Optimum frequency for mixing was found by sweeping the frequency and observing cavitation behavior in the channel. For high-viscosity experiments, the flow rate was fixed at 8  $\mu\text{L}/\text{min}$ .

**Working Mechanism.** The operating mechanism of the acoustofluidic mixing device is shown in Figure 1. The PDMS

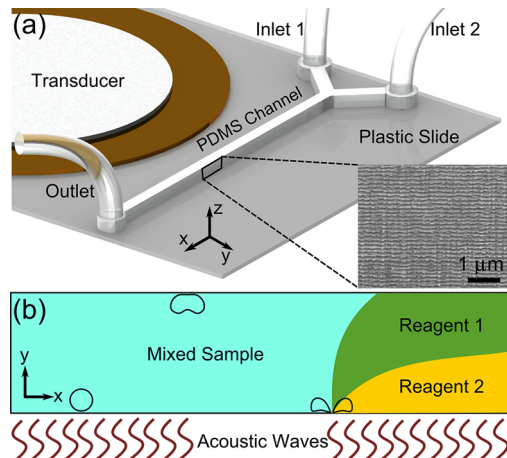


**Figure 1.** (a) Diagram of the microfluidic channel with the SEM image of the silicon master mold. The wavy structures are transferred onto the PDMS channel sidewall. (b) Cartoon representation of the mixing of two reagents when the bubble along the sidewall of the microfluidic channel collapses in the presence of acoustic waves. Two reagents flowing side-by-side in the channel mix by the induced mass transport via the bubble cavitation from the sidewall.

microchannel is made from a silicon mold that is patterned by photoresist followed by DRIE. The DRIE process achieves vertical etching via cycles of etching of silicon and deposition of an inert passivation layer to minimize lateral silicon displacement. The duration of each cycle determines the roughness of the Si channel walls (shorter cycles result in smoother walls). As a result of the DRIE process, the sidewall of the silicon mold features wavy structures (inset in Figure 1a). These wavy structures of the silicon mold are subsequently transferred to

the PDMS channel by the replica-molding process. The rough surface of the PDMS sidewalls develops voids when a liquid is injected into the PDMS channel. These voids form stabilized cavitation nuclei when an acoustic field is applied in the liquid.<sup>60</sup> It was shown that the growth rate of microbubbles depends on the size of the initial nucleation sites.<sup>61</sup> Acoustic waves consist of compression and expansion cycles. During the expansion cycle, the diffusion boundary layer of the bubbles becomes thinner, and the surface area of the bubble gets larger. As a result, gas is transferred into the bubbles from the surrounding fluidic media. Depending on the flow rates and the viscosity of the fluid, we have observed both steady and unsteady cavitation in the devices. With low flow rates, bubbles frequently emerge and disappear from the channel sidewall, suggesting unsteady cavitation. During this process, bubbles grow in expansion cycles until they become unstable and eventually collapse in the next compression cycle.<sup>62</sup> The radius,  $R_c$ , of a single bubble at the collapsing point can be approximated by the Rayleigh-Plesset equation.<sup>63</sup>

The left panel of Figure 2a shows the modes of a single-bubble collapse near a boundary. As the bubble collapses,

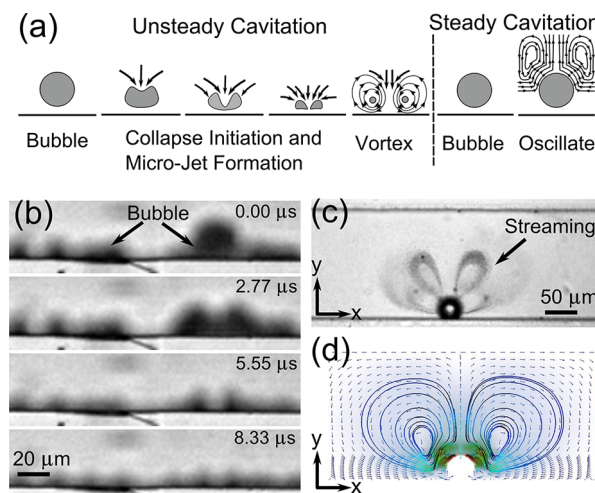


**Figure 2.** (a) Unsteady cavitation (left panel): modes of bubble collapse near a boundary in the presence of acoustic waves. Microjet and counter-rotating vortices are created in the final stages of the collapse. Steady cavitation (right panel): microstreaming phenomenon. (b) Optical images of a bubble's unsteady cavitation captured by the fast camera at 360 000 fps. (c) Optical images of a bubble's steady cavitation captured at 5000 fps (i.e., microstreaming of a bubble visualized by microbeads). (d) Simulated streamlines from theory.

jetting and counter-rotating vortices occur. Versluis et al. estimated the velocity of the jetting water to be on the order of 25 m/s from the cavitation bubble generated by a snapping shrimp.<sup>64</sup> The jetting phenomenon was used in applications such as sonoporation and cavitation-mediated drug delivery.<sup>65</sup> Zwaan et al. estimated that the center of each counter-rotating vortex rotates at a rate of 10 000 rev/s.<sup>66</sup> These fast-rotating vortices break the laminar flow, enabling homogeneous mixing instantaneously. Figure 1b shows a cartoon representation of microfluidic mixing by bubble cavitation from the channel sidewall.

At high flow rates ( $\geq 30 \mu\text{L}/\text{min}$ ), steady cavitation is prevalently observed. During this process, the bubble membranes oscillate vigorously (both harmonics and sub-harmonics are observed), which gives rise to microstream-

ing.<sup>67,68</sup> pressure and velocity fluctuations in the surrounding fluid (Figure 2c and d and the right panel in Figure 2a). The flow patterns in Figure 2d were obtained using an in-house finite element code based on the perturbation approach similar to that used by Köster.<sup>69</sup> The streaming phenomenon breaks the fluidic interface and enhances the mass transport of fluids, thus inducing mixing. It must be noted that the perturbation approach is valid only for slow streaming<sup>70</sup> and should not be used for quantitative comparisons with the experiments that involve large amplitudes of acoustic radiation. However, in the absence of numerical analysis of the so-called fast streaming, the perturbation approach sheds light into acoustic streaming phenomena for qualitative comparisons. At high flow rates, bubbles do not collapse since higher acoustic pressure is needed to counterbalance the rise in pressure associated with fluid flow inside the microchannels.

## RESULTS AND DISCUSSION

To demonstrate the inception and cavitation of bubbles from the PDMS microchannel sidewall, DI water was injected into the channel using a syringe pump (KDS-210, KD Scientific). Figure 2b shows the top view of a bubble-collapsing sequence occurring at the boundary. The bubble grew to a critical size of approximately 20  $\mu\text{m}$  on the sidewall and then collapsed. The critical size is defined by the Rayleigh-Plesset equation<sup>63</sup> and gives the maximum size before the bubbles collapse. Along the channel, as the bubbles collapsed, they were fragmented into tiny bubbles. Due to the smoother surfaces of the top and bottom of the microchannel, bubble inception or cavitation was observed only on the channel sidewalls but not on the top or bottom surfaces. On the basis of atomic force microscopic (AFM) images, the root-mean-square (rms) roughness of the top surface, bottom surface, and sidewalls of the microchannel was determined to be 2.2, 23, and 100 nm, respectively. These results are congruent with the fact that the inception and cavitation of bubbles were observed only from the sidewalls. They also agree well with the report from Arora et al.,<sup>71</sup> which demonstrated cavitation from the corrugated surface of acrylic polymer particles and none from a smooth one.

To demonstrate effective mixing, water and fluorescein dye were injected at the same flow rates inside the microchannel. Figure 3a and b show the side-by-side laminar flow of two fluids at 13  $\mu\text{L}/\text{min}$  in the absence and presence of acoustic waves, respectively. The mixing results were quantitatively studied by measuring the gray scale values of the images, a good indicator of the fluorescein dye concentration in the channel (Figure 3c). The dye concentration profile before and after mixing was measured. The intensity profile shown in Figure 3c indicates no mixing of fluorescein dye and DI water when the acoustic transducer is off. The average intensity of the fluorescein concentration before mixing was measured to be 164.3 arbitrary units. Once the transducer was switched on, bubbles appeared to inception and cavitate from the sidewalls, inducing rapid mixing (Figure 3b) and resulting in a uniform gray scale distribution across the channel width (Figure 3c). Mixing occurs via a combination of steady and unsteady cavitations. The average intensity after mixing was measured to be 87.6 arbitrary units, suggesting homogeneous mixing of the two fluids. The mixing time was estimated from various trials using a fast camera (Fastcam SA4, Photron, at 20 000 frames per second) to be 10 to 50 ms.

During the operation, we also observed microbubbles moving along the microchannel, which contributes to the

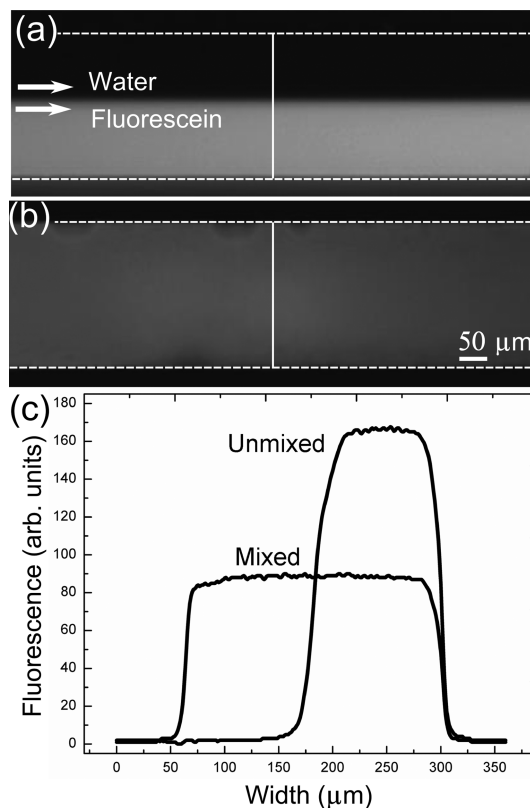


**Figure 3.** (a) Laminar flow of DI water and fluorescein dye in the absence of acoustic waves. (b) Homogenized mixing in the presence of bubble inception and cavitations due to the acoustic field. (c) Fluorescence plot across the channel width (vertical lines in a and b) before and after mixing.

mixing via microstreaming and cavitation of smaller bubbles shooting into the fluid. In Figure 4, a bubble that was generated elsewhere in the channel propelled with the burst of smaller bubble fragments. Depending on the position of these bubble bursts, the bubble moved along the channel in a certain direction. First, it moved upstream with an average velocity about 58 mm/s (Figure 4a–c), then localized with smaller-amplitude movements with constant streaming and cavitation events (Figure 4d), and finally started moving downstream (Figure 4e). These mobile bubbles can enhance the mixing, especially in regions where bubble inception is not frequent. In a bubble cluster, smaller bubble cavitations also contribute to the mixing. Bremond et al. studied bubble–bubble interactions and jetting behavior using an extended Rayleigh-Plesset equation which shows that in the event of bubble cluster cavitations, a jetting flow toward the center of the cluster was generated.<sup>72</sup>

The mixing performance of our acoustofluidic mixing device was further examined using various ratios of DI water and PEG700 solutions. We measured dynamic viscosities of the PEG solutions (Table 1). For all the PEG solutions, the flow rate was fixed at 8  $\mu\text{L}/\text{min}$ . A 67% PEG-water solution (viscosity: 34.2 mPa s) was injected from one inlet and was kept the same for all experiments (Figure 5a–d). The second inlet was used for injecting varying concentrations of PEG solutions. Mixing efficiency ( $M$ ) was calculated according to the following equation:<sup>55</sup>

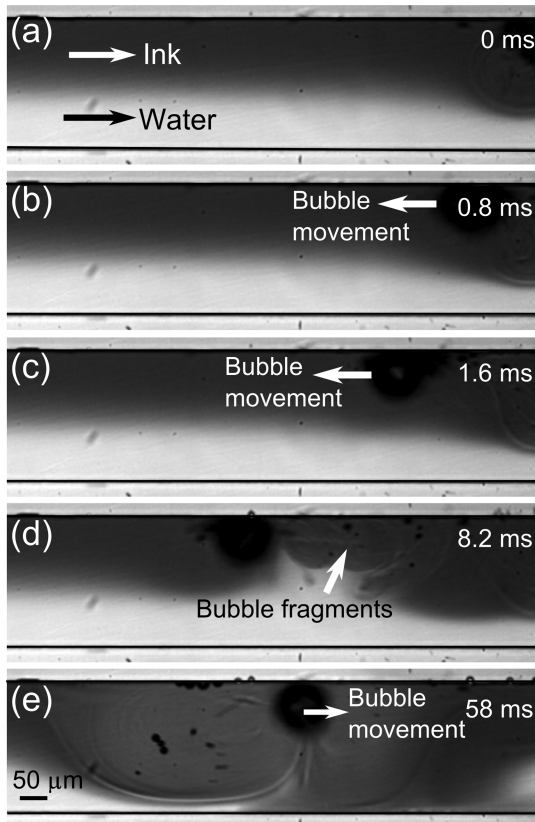


**Figure 4.** (a–d) A microbubble is moving in the channel against the fluid flow via small fragmentations from the right side of the bubble. (e) Acoustic streaming and further smaller bubble cavitations help mixing, and then the bubble propels to the right by fragmentations from the left side of the bubble.

**Table 1. Dynamic Viscosity of DI Water–PEG700 Mixture Solutions at 25 °C<sup>a</sup>**

PEG700 (volume %)	$\mu_2$ (mPa s)	$\mu_{\text{mixed}}$ (mPa s)
50	18.3	21.2
63	24.5	27.9
67	34.2	34.2
71	41.7	37.7
77	48.8	41.7
83	65.3	47.1
90	77.3	48.8
100	95.9	55.8

<sup>a</sup> $\mu_2$  indicates the viscosity of PEG solution with the given concentration injected from the second inlet, and  $\mu_{\text{mixed}}$  indicates the viscosity of the mixed solution.  $\mu_1$  is fixed at 34.2 mPa s.

$$M = 1 - \frac{\sqrt{\frac{1}{n} \sum (I_i - I_m)^2}}{I_m} \quad (1)$$

where  $M$  is the mixing efficiency,  $n$  is the total number of points,  $I_i$  is the intensity at each point, and  $I_m$  is the average intensity. For the perfectly mixed fluids,  $M$  is 1, and for the unmixed fluids,  $M$  is 0. A mixing efficiency of 0.9 or above indicates excellent mixing, and a mixing efficiency between 0.8 and 0.9 indicates acceptable mixing.<sup>55</sup> Figure 5e shows mixing results for eight different viscosity values (50–100% PEG concentration used in the second inlet). As shown in Figure 5b–d, two PEG solutions were mixed with very uniform

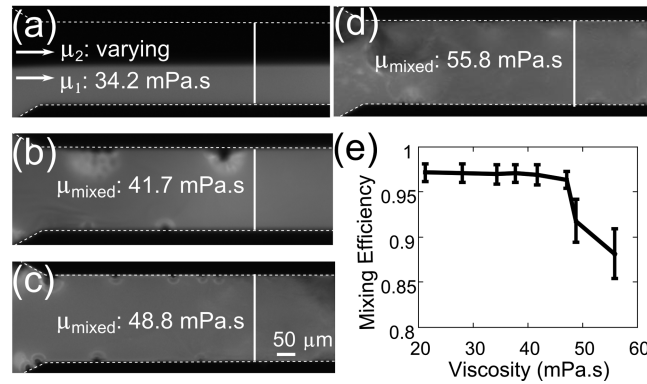


**Figure 5.** (a) Laminar flow of the unmixed PEG solutions where inlet 1 was kept at a constant viscosity of 34.2 mPa s. (b) Mixed solutions with  $\mu_{\text{mixed}}$ : 41.7 mPa s, (c) 48.8 mPa s, and (d) 55.8 mPa s. (e) Plot of the mixing efficiency versus dynamic viscosity. The error bars represent the standard error of the mixing index measurements using different channels.

intensity profiles. Bubbles emerging from the sidewalls are also visible in Figure 5b–d. When we used 90% PEG solution with 77.3 mPa s (86.8 times higher than water) in the second inlet, a mixing efficiency of 0.92 was achieved. Viscosity of the mixture of 67% (in the first inlet) and 90% (in the second inlet) PEG solutions was measured to be 48.8 mPa s, which is 54.9 times higher than the viscosity of water (0.89 mPa s). The Reynolds number for the mixed fluids was calculated to be  $1.14 \times 10^{-2}$ , which is significantly lower than the Reynolds number (e.g., 73.27 in ref 55) reported in the previously reported high-viscosity mixing studies.<sup>54,55</sup> With 100% PEG solution (final mixed viscosity: 55.8 mPa s), the mixing efficiency was 0.88, and the mixing time was less than 100 ms. With its ability to mix highly viscous fluids in microfluidic channels, our acoustofluidic mixer can be valuable in many applications in chemistry and biomedicine. For example, it can be used in sputum analysis for diagnostic purposes. Clinical sputum samples from cystic fibrosis of the pancreas and other pulmonary diseases have a viscosity ranging from 50 to 100 mPa s,<sup>73</sup> which is at a similar range as those used in our acoustofluidic micromixers.

## CONCLUSIONS

In conclusion, we have demonstrated an acoustofluidic mixer that can effectively mix two highly viscous fluids within 100 ms. The mixing was achieved by using the surface roughness of PDMS channel sidewalls to inception and cavitate bubbles in the presence of acoustic waves. Large bubbles developed in the channel were found to be propelled via small bubble cavitations, which also contributed to the mixing. Mixing performance of the device was tested using a range of PEG solutions with different viscosities, and the mixing efficiency was measured to be 0.88–0.97. When 90% PEG (77.3 mPa s) solution and 67% PEG-fluorescein (34.2 mPa s) solution were co-injected into the device, a mixing efficiency of 0.92 was achieved. The viscosity of the mixed solution was measured to be 48.8 mPa s (54.9 times higher than that of water), and the Reynolds number was ~0.01, which is 2–3 orders of magnitude lower than those reported in previous micromixers.<sup>54,55</sup> Our device is simple to fabricate, easy to operate, and can be conveniently integrated with other microfluidic components. With further optimization, we believe that our acoustofluidic

micromixer has great potential in many lab-on-a-chip applications such as medical diagnostics, nanoparticle synthesis, microscopic sonochemical reactions, and biochemical reactors.

## ■ ASSOCIATED CONTENT

### Supporting Information

Figure S-1 shows homogeneous mixing in the different planes along the *z* direction. This material is available free of charge via the Internet at <http://pubs.acs.org>.

## ■ AUTHOR INFORMATION

### Corresponding Author

\*E-mail: junhuang@psu.edu.

### Notes

The authors declare no competing financial interest.

## ■ ACKNOWLEDGMENTS

We thank Dr. Bala K. Juluri, Dr. Yuebing Zheng, and Mr. Joseph Rufo for help with the manuscript. This research was supported by National Institutes of Health (Director's New Innovator Award, 1DP2OD007209-01), American Asthma Foundation Scholar Award, and the Penn State Center for Nanoscale Science (MRSEC) under grant DMR-0820404. Components of this work were conducted at the Penn State node of the NSF-funded National Nanotechnology Infrastructure Network.

## ■ REFERENCES

- (1) Song, Y.; Hormes, J.; Kumar, C. S. S. R. *Small* **2008**, *4*, 698–711.
- (2) Dendukuri, D.; Pregibon, D. C.; Collins, J.; Hatton, T. A.; Doyle, P. S. *Nat. Mater.* **2006**, *5*, 365–369.
- (3) Yang, S.; Guo, F.; Kiraly, B.; Mao, X.; Lu, M.; Leong, K. W.; Huang, T. *J. Lab Chip* **2012**, *12*, 2097–2102.
- (4) Pollack, L.; Tate, M. W.; Darnton, N. C.; Knight, J. B.; Gruner, S. M.; Eaton, W. a; Austin, R. H. *Proc. Natl. Acad. Sci. U. S. A.* **1999**, *96*, 10115–10117.
- (5) Xie, Y.; Ahmed, D.; Lapsley, M. I.; Lin, S. S.; Nawaz, A. A.; Wang, L.; Huang, T. *J. Anal. Chem.* **2012**, *84*, 7495–7501.
- (6) Schabas, G.; Yusuf, H.; Moffitt, M. G.; Sinton, D. *Langmuir* **2008**, *24*, 637–643.
- (7) Chisolm, C. N.; Evans, C. R.; Jennings, C.; Black, W. A.; Antosz, F. J.; Qiang, Y.; Diaz, A. R.; Kennedy, R. T. *J. Chromatogr. A* **2010**, *1217*, 7471–7477.
- (8) Hung, L.-Y.; Chuang, Y.-H.; Kuo, H.-T.; Wang, C.-H.; Hsu, K.-F.; Chou, C.-Y.; Lee, G.-B. *Biomed. Microdevices* **2013**, *15*, 339–352.
- (9) Hong, J. W.; Studer, V.; Hang, G.; Anderson, W. F.; Quake, S. R. *Nat. Biotechnol.* **2004**, *22*, 435–439.
- (10) Gorkin, R.; Park, J.; Siegrist, J.; Amasia, M.; Lee, B. S.; Park, J.-M.; Kim, J.; Kim, H.; Madou, M.; Cho, Y.-K. *Lab Chip* **2010**, *10*, 1758–1773.
- (11) Thom, J.; Ivey, L.; Eikelboom, J. *J. Thromb. Haemostasis* **2003**, *1*, 2689–2691.
- (12) Lu, X.; Samuelson, D. R.; Xu, Y.; Zhang, H.; Wang, S.; Rasco, B. A.; Xu, J.; Konkel, M. E. *Anal. Chem.* **2013**, *85*, 2320–2327.
- (13) Oh, B.-R.; Huang, N.-T.; Chen, W.; Seo, J. H.; Chen, P.; Cornell, T. T.; Shanley, T. P.; Fu, J.; Kurabayashi, K. *ACS Nano* **2014**, in print.
- (14) Dishinger, J. F.; Reid, K. R.; Kennedy, R. T. *Anal. Chem.* **2009**, *81*, 3119–3127.
- (15) Shamsi, M. H.; Choi, K.; Ng, A. H. C.; Wheeler, A. R. *Lab Chip* **2013**, *14*, 547–554.
- (16) Xie, Y.; Todd, N. W.; Liu, Z.; Zhan, M.; Fang, H.; Peng, H.; Alattar, M.; Deepak, J.; Stass, S. A.; Jiang, F. *Lung Cancer* **2010**, *67*, 170–176.
- (17) Krausz, C. *Best Pract. Res., Clin. Endocrinol. Metab.* **2011**, *25*, 271–285.
- (18) Whitesides, G. M. *Nature* **2006**, *442*, 368–373.
- (19) Song, H.; Ismagilov, R. F. *J. Am. Chem. Soc.* **2003**, *125*, 14613–14619.
- (20) Zhao, C.; Liu, Y.; Zhao, Y.; Fang, N.; Huang, T. *J. Nat. Commun.* **2013**, *4*, 2305.
- (21) Mao, X.; Huang, T. *J. Lab Chip* **2012**, *12*, 1412–1416.
- (22) Mao, X.; Huang, T. *J. Lab Chip* **2012**, *12*, 4006–4009.
- (23) Mao, X.; Juluri, B. K.; Lapsley, M. I.; Stratton, Z. S.; Huang, T. *J. Microfluid. Nanofluidics* **2009**, *8*, 139–144.
- (24) Mao, X.; Waldeisen, J. R.; Huang, T. *J. Lab Chip* **2007**, *7*, 1260–1262.
- (25) Hashmi, A.; Yu, G.; Reilly-Collette, M.; Heiman, G.; Xu, J. *J. Lab Chip* **2012**, *12*, 4216–4227.
- (26) Ahmed, D.; Chan, C. Y.; Lin, S.-C. S.; Muddana, H. S.; Nama, N.; Benkovic, S. J.; Huang, T. *J. Lab Chip* **2013**, *13*, 328–331.
- (27) Kakuta, M.; Jayawickrama, D. A.; Wolters, A. M.; Manz, A.; Sweedler, J. V. *Anal. Chem.* **2003**, *75*, 956–960.
- (28) Guo, F.; Lapsley, M. I.; Nawaz, A. A.; Zhao, Y.; Lin, S. S.; Chen, Y.; Yang, S.; Zhao, X.; Huang, T. *J. Anal. Chem.* **2012**, *84*, 10745–10749.
- (29) Miller, E. M.; Wheeler, A. R. *Anal. Bioanal. Chem.* **2009**, *393*, 419–426.
- (30) Hsu, C.-H.; Folch, A. *Appl. Phys. Lett.* **2006**, *89*, 144102.
- (31) Stroock, A. D.; Dertinger, S. K. W.; Ajdari, A.; Mezic, I.; Stone, H. A.; Whitesides, G. M. *Science* **2002**, *295*, 647–651.
- (32) Therriault, D.; White, S. R.; Lewis, J. A. *Nat. Mater.* **2003**, *2*, 265–271.
- (33) Neils, C.; Tyree, Z.; Finlayson, B.; Folch, A. *Lab Chip* **2004**, *4*, 342–350.
- (34) Sheng, W.; Ogunwobi, O. O.; Chen, T.; Zhang, J.; George, T. J.; Liu, C.; Fan, Z. H. *Lab Chip* **2014**, *14*, 89–98.
- (35) Mei, Q.; Xia, Z.; Xu, F.; Soper, S. a; Fan, Z. H. *Anal. Chem.* **2008**, *80*, 6045–6050.
- (36) Tsai, J.; Lin, L. *Sens. Actuators, A* **2002**, *97–98*, 665–671.
- (37) Hellman, A. N.; Rau, K. R.; Yoon, H. H.; Bae, S.; Palmer, J. F.; Phillips, K. S.; Allbritton, N. L.; Venugopalan, V. *Anal. Chem.* **2007**, *79*, 4484–4492.
- (38) Ryu, K. S.; Shaikh, K.; Goluch, E.; Fan, Z.; Liu, C. *Lab Chip* **2004**, *4*, 608–613.
- (39) Riahi, M.; Alizadeh, E. *J. Micromech. Microeng.* **2012**, *22*, 115001.
- (40) Chang, C.-C.; Yang, R.-J. *Microfluid. Nanofluid.* **2007**, *3*, 501–525.
- (41) Harnett, C. K.; Templeton, J.; Dunphy-Guzman, K. a; Senousy, Y. M.; Kanouff, M. P. *Lab Chip* **2008**, *8*, 565–572.
- (42) Sigurdson, M.; Wang, D.; Meinhart, C. D. *Lab Chip* **2005**, *5*, 1366–1373.
- (43) Thorsen, T.; Maerkli, S. J.; Quake, S. R. *Science* **2002**, *298*, 580–584.
- (44) Park, H. Y.; Qiu, X.; Rhoades, E.; Korlach, J.; Kwok, L. W.; Zipfel, W. R.; Webb, W. W.; Pollack, L. *Anal. Chem.* **2006**, *78*, 4465–4473.
- (45) Yaralioglu, G. G.; Wygant, I. O.; Marentis, T. C.; Khuri-Yakub, B. T. *Anal. Chem.* **2004**, *76*, 3694–3698.
- (46) Yang, Z.; Matsumoto, S.; Goto, H.; Matsumoto, M.; Maeda, R. *Sens. Actuators, A* **2001**, *93*, 266–272.
- (47) Wixforth, A.; Strobl, C.; Gauer, C.; Toegl, a; Scriba, J.; v Guttenberg, Z. *Anal. Bioanal. Chem.* **2004**, *379*, 982–991.
- (48) Frommelt, T.; Kostur, M.; Wenzel-Schäfer, M.; Talkner, P.; Hänggi, P.; Wixforth, A. *Phys. Rev. Lett.* **2008**, *100*, 034502.
- (49) Tseng, W.-K.; Lin, J.-L.; Sung, W.-C.; Chen, S.-H.; Lee, G.-B. *J. Micromech. Microeng.* **2006**, *16*, 539–548.
- (50) Huang, P.-H.; Xie, Y.; Ahmed, D.; Rufo, J.; Nama, N.; Chen, Y.; Chan, C. Y.; Huang, T. *J. Lab Chip* **2013**, *13*, 3847–3852.
- (51) Ahmed, D.; Mao, X.; Shi, J.; Juluri, B. K.; Huang, T. *J. Lab Chip* **2009**, *9*, 2738–2741.
- (52) Ahmed, D.; Mao, X.; Juluri, B. K.; Huang, T. *J. Microfluid. Nanofluid.* **2009**, *7*, 727–731.
- (53) Liu, R. H.; Yang, J.; Pindera, M. Z.; Athavale, M.; Grodzinski, P. *Lab Chip* **2002**, *2*, 151–157.

- (54) Wang, S.; Huang, X.; Yang, C. *Lab Chip* **2011**, *11*, 2081–2087.
- (55) Li, Y.; Xu, Y.; Feng, X.; Liu, B. *Anal. Chem.* **2012**, *84*, 9025–9032.
- (56) Bruus, H.; Dual, J.; Hawkes, J.; Hill, M.; Laurell, T.; Nilsson, J.; Radel, S.; Sadhal, S.; Wiklund, M. *Lab Chip* **2011**, *11*, 3579–3580.
- (57) Lin, S.-C. S.; Mao, X.; Huang, T. J. *Lab Chip* **2012**, *12*, 2766–2770.
- (58) Friend, J.; Yeo, L. Y. *Rev. Mod. Phys.* **2011**, *83*, 647–704.
- (59) Qin, D.; Xia, Y.; Whitesides, G. M. *Nat. Protoc.* **2010**, *5*, 491–502.
- (60) Marschall, H. B.; Mørch, K. a.; Keller, a. P.; Kjeldsen, M. *Phys. Fluids* **2003**, *15*, 545.
- (61) Shpak, O.; Stricker, L.; Versluis, M.; Lohse, D. *Phys. Med. Biol.* **2013**, *58*, 2523–2535.
- (62) Pradhan, A.; Jones, R. C.; Caruntu, D.; O'Connor, C. J.; Tarr, M. a. *Ultrason. Sonochem.* **2008**, *15*, 891–897.
- (63) Shima, A. *Shock Waves* **1997**, *7*, 33–42.
- (64) Versluis, M.; Schmitz, B.; von der Heydt, A.; Lohse, D. *Science* **2000**, *289*, 2114–2117.
- (65) Ohl, C.-D.; Arora, M.; Ikink, R.; de Jong, N.; Versluis, M.; Delius, M.; Lohse, D. *Biophys. J.* **2006**, *91*, 4285–4295.
- (66) Zwaan, E.; Le Gac, S.; Tsuji, K.; Ohl, C.-D. *Phys. Rev. Lett.* **2007**, *98*, 254501.
- (67) Marmottant, P.; Hilgenfeldt, S. *Proc. Natl. Acad. Sci. U. S. A.* **2004**, *101*, 9523–9527.
- (68) Wiklund, M.; Green, R.; Ohlin, M. *Lab Chip* **2012**, *12*, 2438–2451.
- (69) Köster, D. *Numerical Simulation of Acoustic Streaming on SAW-Driven Biochips*; University of Augsburg: Augsburg, Germany, 2006.
- (70) Ding, X.; Li, P.; Lin, S.-C. S.; Stratton, Z. S.; Nama, N.; Guo, F.; Slotcavage, D.; Mao, X.; Shi, J.; Costanzo, F.; Huang, T. J. *Lab Chip* **2013**, *13*, 3626–3649.
- (71) Arora, M.; Ohl, C.-D.; Mørch, K. *Phys. Rev. Lett.* **2004**, *92*, 174501.
- (72) Bremond, N.; Arora, M.; Ohl, C.-D.; Lohse, D. *Phys. Rev. Lett.* **2006**, *96*, 224501.
- (73) Feather, E. A.; Russell, G. *Br. J. Dis. Chest* **1970**, *64*, 192–200.